GEOPHYSICS, VOL. 77, NO. 4 (JULY-AUGUST 2012); P. R175–R187, 11 FIGS., 1 TABLE.
10.1190/GEO2011-0291.1

Estimation of free gas saturation from seismic reflection surveys by the genetic algorithm inversion of a P-wave attenuation model

Eugene C. Morgan[1], Maarten Vanneste[2], Isabelle Lecomte[3], Laurie G. Baise[1], Oddvar Longva[4], and Brian McAdoo[5]

ABSTRACT

Many previously proposed methods of estimating free gas saturation from seismic survey data rely on calibration to invasively collected, in situ measurements. Typically, such in situ measurements are used to parameterize or calibrate rock-physics models, which can then be applied to seismic data to achieve saturation estimates. We tested a technique for achieving estimates of the spatial distribution of gas saturation solely from shipboard seismic surveys. We estimated the quality factor from seismic reflection surveys using the spectral ratio method, and then inverted a mesoscopic-scale P-wave attenuation model to find the parameters that matched the modeled attenuation to our estimates of observed attenuation within the range of seismic frequencies. By using a genetic algorithm for this inversion, we not only searched efficiently for a global solution to the nonlinear set of equations that compose the model, but also constrain the search to a relatively broad set of realistic parameter values. Thus, our estimates do not rely on in situ measurements of these parameters, but on distributions of their possible values, many of which may be referenced from literature. We first tested this method at Blake Ridge, offshore North and South Carolina, where an approximately 400-m-deep gas-saturated zone underlies a field of methane hydrates. The extensive field work and subsequent studies at this site make it ideal for validating our method. We also demonstrated the applicability of our method to shallower deposits by presenting results from Finneidfjord, Norway, where the inversion of the P-wave attenuation model recognizes very small gas saturations.

INTRODUCTION

Accurately quantifying the amount of free gas in a given geologic layer is not only of interest for resource exploration and reservoir characterization, but also for slope stability analysis and carbon sequestration. Marine sediments frequently contain undissolved gas bubbles, typically methane, of biogenic or thermogenic origins (Sills et al., 1991). Large fields of free methane gas lie trapped beneath gas hydrates, associated with bottom-simulating reflectors (BSR) (Bangs et al., 1993; Holbrook et al., 1996; Dickens et al., 1997; Wood, 2000; Lee, 2004; Haacke et al., 2007; Horozal et al., 2009). Also, shallow near-shore sediments rich in organic material commonly contain gas bubbles (Urgeles et al., 2007; Seifert et al., 2008). Free-gas bubbles can significantly change the behavior of submarine soils, impacting offshore construction and, potentially, increasing landslide hazard (Kayen and Lee, 1993; McAdoo et al., 2000, 2004; Sultan et al., 2004; Berndt et al., 2005; Xu and Germanovich, 2006). In the submarine environment, gas-charged sediments cover large areas, and most current methods of estimating gas saturations in these sediments only do so at discrete points where in situ measurements exist. These in situ methods are time-consuming and cumbersome. Many previous studies that use seismic data to estimate the distribution of gas concentration rely on calibration to in situ measurements (e.g., Holbrook et al., 1996; Dickens et al., 1997; Lu and McMechan, 2002, 2004; Lee, 2004).

Manuscript received by the Editor 2 August 2011; revised manuscript received 5 January 2012; published online 18 June 2012.
[1]Tufts University, Department of Civil and Environmental Engineering, Medford, Massachusetts, USA. E-mail: eugene.morgan@duke.edu; laurie.baise@tufts.edu.
[2]NGI, Oslo, Norway and ICG, Oslo, Norway. E-mail: maarten.vanneste@ngi.no.
[3]NORSAR, Kjeller, Norway and ICG, Oslo, Norway. E-mail: isabelle@norsar.no.
[4]NGU, Trondheim, Norway and ICG, Oslo, Norway. E-mail: oddvar.longva@ngu.no.
[5]Vassar College, Department of Earth Science and Geography, Poughkeepsie, New York, USA. E-mail: brmcadoo@vassar.edu.

In this paper, we illustrate a method of estimating the gas saturation (S_g) of charged sediments that relies only on seismic data and literature constraints for the physical parameters. The goal of this study is to make seismic surveying a time-efficient way of obtaining preliminary and reliable estimates for the distribution of free gas over large areas.

Intrusive methods of detecting free gas and measuring its saturation include identifying drastic decreases in P-wave velocity (V_P) from vertical seismic profiling (VSP) (Holbrook et al., 1996), examining well-log velocities for $V_P/V_S < 2.0$ (Lee, 2004; Lee and Collett, 2009), correlation with resistivity logs (Archie, 1942; Collett and Ladd, 2000; Lu and McMechan, 2002), and pressure core sampling (Dickens et al., 1997). In general, these methods are costly, time-consuming, and spatially limited. Additionally, they are not necessarily sensitive to small concentrations of gas. For instance, Lee and Collett (2009) note that examining well-log velocities for $V_P/V_S < 2.0$ does not work well for low gas saturations.

However, Lee and Collett (2009) note that for low gas saturations, high levels of P-wave attenuation can occur within the range of seismic frequencies and not within logging frequencies, illustrating the utility of seismic surveys in detecting partially gas-saturated sediments. Additionally, it is widely believed that free gas causes the BSR. Free gas tends to produce a distinct high-amplitude, polarity-reversed reflection (characteristic of the BSR) sometimes followed by amplitude blanking (or "gas-blanking") in seismic reflection profiles (Bangs et al., 1993; Best et al., 2003; Seifert et al., 2008). The negative polarity of this reflection indicates that the layer below has less acoustic impedance (the product of density and velocity) than the layer above the BSR, and the amplitude of the reflection is largely controlled by free gas (Trehu et al., 2003; Bangs et al., 1993). Although the presence of free gas may not always produce a bottom-simulating reflection, mapping the extent of any such reflection serves as a reasonable proxy for mapping the distribution of trapped free gas (e.g., Bünz et al., 2005), where more strongly negative reflection coefficients of the BSR indicate the presence of underlying free gas with more certainty (Best et al., 2003; Trehu et al., 2003). As an instance of looking at the more complex geometry of such gas-bearing layers, Trehu and Flueh (2001) constrain the distribution and thickness of the free gas zone at Hydrate Ridge (offshore Oregon) from low velocities and high attenuation determined from refraction seismic surveys.

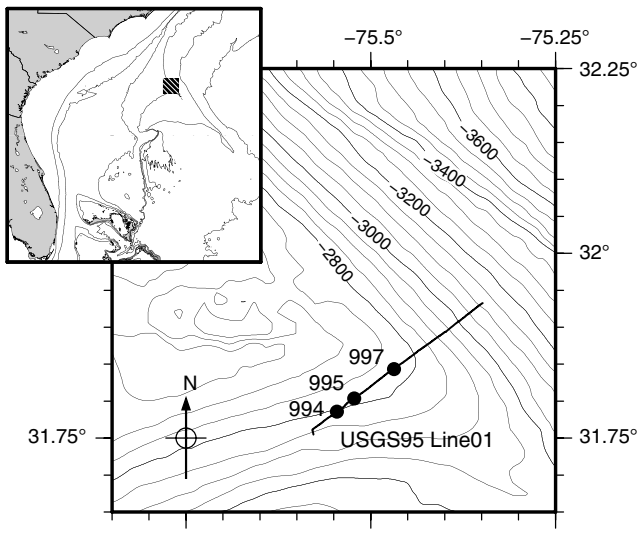

Figure 1. Location map of Blake Ridge with navigation of the seismic profile used in this study (USGS Line 01) and ODP leg 164, holes 994, 995, and 997.

In terms of estimating S_g, shipboard seismic surveys serve as an attractive alternative to the intrusive methods listed above because of their relative ease of deployment, cost effectiveness, and wide spatial coverage, but many studies that utilize seismic surveys rely on calibration at boreholes. For example, at Blake Ridge (Figure 1), Lu and McMechan (2002) use seismic profiling to predict gas saturations in between boreholes by calibrating acoustic impedance to water-filled porosity at the boreholes. In a later study at the same location, Lu and McMechan (2004) use these same calibrations in conjunction with the elastic impedance inversion of a nearby multichannel seismic line to estimate free gas concentrations. Several studies use seismic velocities to estimate gas saturation, and some of these studies make little or no use of borehole or coring measurements. Using ocean-bottom seismometer and cable data, Bünz et al. (2005) estimate free gas concentration by means of P- and S-wave velocity analysis. Tinivella and Lodolo (2000) and Tinivella and Accaino (2000) estimate free gas concentrations by comparing velocity profiles obtained by inversion of multichannel seismic data to theoretical profiles calculated using either borehole measurements or literature reference values, respectively. Without relying on in situ measurements, Ecker et al. (2000) invert a rock-physics model to estimate gas hydrate and free gas concentrations from interval velocities obtained from AVO analysis of multichannel seismic data collected at Blake Ridge. However, Ecker et al. (2000) note that their saturation estimates show extreme sensitivity to their velocity-interval values, and, in a different study, Zillmer (2006) concludes that small uncertainties in seismic velocities can lead to large variances in gas saturation estimates.

Attenuation and velocity dispersion have a strong dependence on the hydraulic properties of partially saturated media, including gas saturation (White, 1975), whereas velocity depends heavily on other additional physical properties, such as density. Thus, rock-physics models dealing with the attenuation of seismic waves through partially saturated media, such as White's model, may be better suited to invert for gas saturation than velocity models because of the stronger relationship between gas saturation and attenuation. This strong relationship arises from the mechanism of wave-induced fluid flow, where the passage of a fast P-wave through a partially saturated porous medium generates differential fluid pressure between the gas and water, resulting in fluid flow and a slow P-wave, as explained by Biot's theory of wave propagation (Biot, 1962). Energy conversion to this slow-wave mode, and subsequent diffusion of this wave away from the gas-water interface causes significant attenuation of the P-wave within the seismic frequency range. Müller et al. (2010) provide an excellent review of these concepts.

Many models describe the role of fluid flow in attenuation at different scales, but the mesoscopic-scale models (as opposed to micro- and macroscopic-scale models) show the greatest success in reproducing the observed level of attenuation at seismic frequencies (Pride et al., 2004). Here, "mesoscopic" refers to inhomogeneities much larger than grain sizes and much smaller than the wavelength. Carcione and Picotti (2006) adopt the model of White (1975) to functionally relate S_g (as well as many other parameters) to quality factor

(Q, which is inversely proportional to the attenuation factor) within a periodic layered system and use this model to investigate the effect of mesoscopic-scale (free gas) inhomogeneities on attenuation. Furthermore, Carcione and Picotti (2006) assert that the mesoscopic mechanism is largely responsible for losses below the BSR. It should be noted that although this model assumes periodic layering of the inhomogeneities, Dutta and Seri (1979) suggest that the configuration of the gas inclusions has little effect on the attenuation. Thus, (periodic) layering should adequately capture the attenuating behavior of soil with gas bubbles or patchy saturation.

In this paper, we present a method for estimating free gas saturation S_g from seismic reflection data that takes advantage of the strong dependency between gas saturation and attenuation. We do so by inverting the P-wave attenuation model of Carcione and Picotti (2006) (which is the model of White (1975) under periodic layering) to match measured values of Q. Using a genetic algorithm not only allows us to efficiently invert this nonlinear model, but it also lets us constrain the global parameter space to a range of realistic conditions. Thus, we do not need precise values for the input parameters, and, using data from Blake Ridge (Figure 1), we show that reasonable estimates of gas saturation can be achieved without borehole measurements. Here, we generate our estimates of S_g using only input data available from the seismic reflection data and literature values or empirical relationships, and reserve the borehole data at Blake Ridge to validate our method. Our estimates agree not only with these in situ measurements, but also with estimates of S_g from previous studies. We also show that this method is sensitive to environments with very low amounts of free gas by performing the inversion at Finneidfjord, Norway (Figure 2), where shallow free gas deposits may have played a role in a devastating landslide in 1996 and possibly older landslides evident in the bathymetry data from the fjord.

DATA

The data set from Blake Ridge used in this paper contains one single-channel seismic (SCS) line (USGS Line 01; collected in 1995) and three boreholes (994, 995, and 997 from ODP Leg 164; collected in 1995), which lie directly on the seismic profile. From these boreholes, we use the resistivity logs to validate our S_g estimates.

The Finneidfjord data set consists of a grid of 2D seismic lines collected in 2006 (Figure 2). The air-gun source operated at relevant frequencies between 40 and 500 Hz, whereas receivers towed on a single-channel streamer at near-zero offset sampled at ~2600 Hz. A hammer-driven corer collected four 4–5-m-long cores from the Finneidfjord seabed: two within the gas zone, and two on the slopes to the north of the gas zone. A Geotek MSCL device logged the cores after being X-rayed, and subsequent grain-size distribution analyses were performed. Although this location does not host gas hydrates, the seismic profiles display a bottom-simulating reflection (which is high-amplitude, reverse-polarity, and produces signal blanking, but does not parallel the seafloor bottom), and is collocated with the presence of free gas bubbles observed in X-rays of one core (Best et al., 2003).

METHODS

This section outlines our method for (first) estimating Q from our seismic data sets, and (second) inverting the P-wave attenuation model of Carcione and Picotti (2006) to transform these Q estimates ($\hat{Q}$) into estimates of gas saturation S_g. It is important to note that we only use the seismic profiles and literature knowledge of geologic properties to yield our S_g estimates, and that no calibration to logging or core data is necessary to produce our estimates. These in situ measurements are reserved for validation at the Blake Ridge site, and should be noted that having such measurements for comparison is always advisable. We then fit the model of Carcione and Picotti (2006) to our estimates of attenuation using our best constraints on all the variables for this model (i.e., the most likely parameters based on our prior knowledge).

Seismic data preprocessing

To get the best quality data for measuring attenuation, all seismic data underwent some basic processing steps to reduce noise and provide the most appropriate reflection amplitudes. We performed amplitude gain correction on all traces to correct for spherical spreading of the seismic wave with depth. Also, we corrected for multiple attenuation in the Finneidfjord seismic profiles via f-k filtering; this procedure was not necessary at the deeper seismic sections from Blake Ridge. Band-pass filtering removed some high-frequency noise from the seismic profiles as well. The band-pass filter for the Blake Ridge data used corner frequencies of 10, 20, 120, and 150 Hz, whereas the filter for the Finneidfjord data had 20, 40, 500, and 600 Hz corner frequencies.

We select an upper portion of the free gas zone at each site to be analyzed because free gas migrates upward, and so this upper portion will likely have the highest gas saturation and pressure, and thus be of most interest. We use either the BSR (Blake Ridge) or the high-amplitude, reverse-polarity reflection (Finneidfjord) to guide our pick of the top of the gas layer, because this represents the shallowest limit of free gas (Holbrook et al., 1996) and is easily identifiable. We pick this horizon using a windowed trough amplitude search, because this reflection is reverse polarity. To mitigate interference (amplitude tuning) with the top horizon and to allow enough time separation for attenuation to occur, we choose the bottom horizon to be twice the period of the lowest frequency below the top:

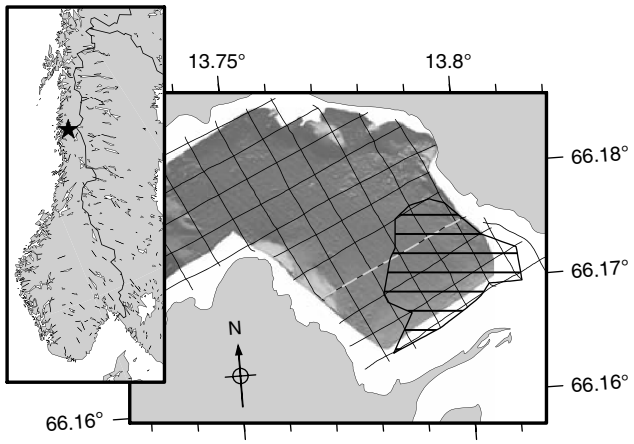

Figure 2. Location map for Finneidfjord, Norway. Thin black lines show navigation of SCS profiling carried out in 2006, and the thick black hatched polygon represents the mapped extent of the bottom-simulating reflection (interpreted as lateral distribution of the free gas zone). Line 08 (used in the analysis here) is marked with the dashed gray line.

$$t_{\text{bottom}} = t_{\text{top}} - \frac{2}{f_{\min}}, \quad (1)$$

where t is two-way traveltime, and $f_{\min} = 20$ Hz and 40 Hz for Blake Ridge and Finneidfjord, respectively. Thus, assuming $V_P = 1500$ m/s, our layer thicknesses are 75 and 37.5 m, respectively, which correspond to one wavelength of the lowest frequency. Holbrook et al. (1996) estimate the thickness of the free gas zone at Blake Ridge to be at least 250 m.

Measuring attenuation

The effective (or apparent) quality factor Q_{eff} of a geologic medium depends not only on intrinsic effects Q_i such as fluid flow, to which free gas plays a significant role, but also on scattering Q_{sc} resulting from the geometry of reflectors and heterogeneities in the layer, to which gas inclusions may also contribute:

$$\frac{1}{Q_{\text{eff}}} = \frac{1}{Q_i} + \frac{1}{Q_{\text{sc}}} \quad (2)$$

(Spencer et al., 1982). It is often difficult to separate scattering effects from intrinsic attenuation, and measurements of attenuation from seismic data frequently report Q_{eff} (e.g., Wood, 2000; Payne et al., 2007; Reine et al., 2009). At Blake Ridge and Finneidfjord, we do not expect a significant level of scattering attenuation (at least within lower frequencies that contain most of the seismic energy) from the gas heterogeneities. The scattering relaxation frequency (f_s) is given by

$$f_s = \frac{V_P}{2\pi h}, \quad (3)$$

where h is the average thickness of the heterogeneities (Gurevich et al., 1997). Assuming $V_P = 1500$ m/s, h has to be at least 3 m to produce $f_s < 100$ Hz, whereas we expect gas inclusions to be on the order of millimeter-to-decimeter scale (Carcione and Picotti, 2006; Haacke et al., 2007). There does exist the potential for the spacing of these thin inclusions to be 3 m or more, which would produce scattering attenuation. We can verify from cores that this is not the case at Finneidfjord, but logging data are not finely resolved enough to refute this source of scattering at Blake Ridge. As a further argument, Sams et al. (1997) find, with some uncertainty, that intrinsic attenuation dominates the effective attenuation over the seismic frequency band. We assume Q_{eff} approximates Q_i, and we refer to these approximations as Q in the rest of the paper.

Methods of measuring Q include: spectral ratio (Stainsby and Worthington, 1985; Payne et al., 2007), frequency shift (Quan and Harris, 1997), centroid of scale (Li et al., 2006), and spectral correlation (Yang and Gao, 2008). Reine et al. (2009) compare different time-frequency transforms in estimating Q under the spectral ratio method and find that using the wavelet transform reduces the sensitivity to the choice of regression bandwidth. At Blake Ridge and Finneidfjord, we estimate Q using the spectral ratio method, where the amplitude spectra at the top and bottom horizons picked in the previous paragraph are found via continuous wavelet transformation, as is done in Reine et al. (2009). We perform the wavelet transformation at each seismic shotpoint because we expect the amount of gas to vary laterally across the gas-bearing layers, and so want to quantify the associated change in Q. Although our attenuation model assumes a layered medium, we can apply this model independently at each location because the single-channel surveys considered in this paper gather the seismic traces at each location independently. Although the methodology herein relies on single-channel data, it could be possible to modify the application of the attenuation model for different forms of seismic exploration. We increase the signal-to-noise ratio (S/N) by flattening the seismic profiles at the seafloor reflection, and then stacking each trace with its neighboring 20 traces (10 on each side; see Figure 3a for an example). The flattening and stacking also produce more smoothly varying Q estimates across each profile because these procedures reduce the effect of singular noisy traces in the profile. We use a brute stack (boxcar weighting), but we realize that other weighting options could be considered, e.g., a Gaussian-weighted stack to emphasize local effects within a given spatial scale. However, we do not expect that minor changes in the weighting strategy would drastically affect our estimates of Q; the brute stack will give a marginally smoother distribution of Q than the Gaussian-weighted stack. The continuous wavelet transformation,

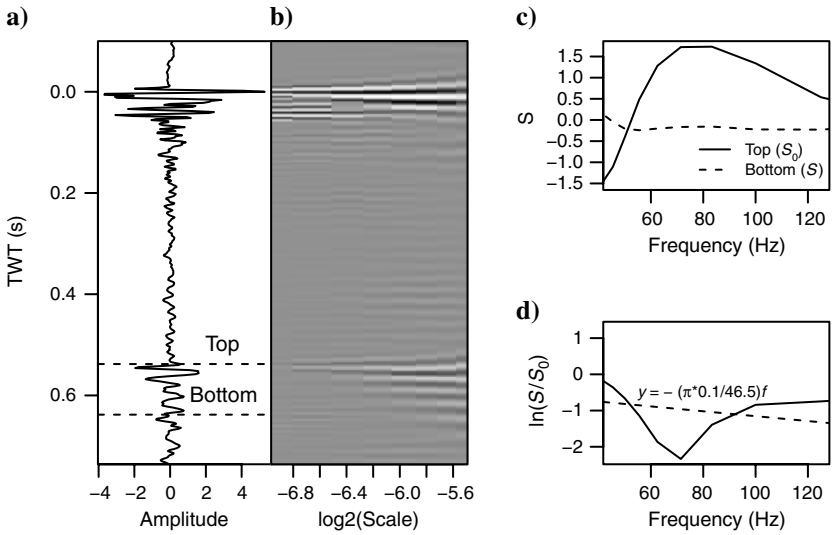

Figure 3. An example of the estimation procedure for $\hat{Q}$, with (a) showing trace 869 after flattening at the seafloor and stacking with 10 neighboring traces on each side, (b) showing the wavelet transform of this trace, (c) showing the spectra extracted from the top and bottom horizons, and (d) plotting the natural log of the ratio of these spectra. The dashed line in (d) is the line fit by least-squares, yielding the $\hat{Q} = 46.5$ in the denominator of the slope.

$$S(\tau, a) = \frac{1}{\sqrt{a}} \int_{-\infty}^{\infty} s(t) \Psi^* \left(\frac{t - \tau}{a} \right) dt, \quad (4)$$

decomposes a signal $s(t)$ into the time-scale domain, where scale a is inversely proportional to frequency, and the coefficients in this domain (the shading in Figure 3b) correspond to the amount of correlation between the signal and the chosen wavelet filter Ψ, and τ is the time offset to the center of the wavelet filter. For all transformations, we use the Morlet wavelet,

$$\Psi(t) = \pi^{-1/4} e^{-i\sigma t} e^{-t^2/2}, \quad (5)$$

with a frequency shift of $\sigma = 5$ (Percival and Walden, 2000). The wavelet transformation provides better time localization in the traveltime domain than time-windowing methods, which becomes of critical importance in dealing with the high-resolution seismic data from Finneidfjord. This issue of time localization is less important at Blake Ridge, where the gas-bearing layer is much thicker than that at Finneidfjord.

Extracting the spectra for the top $S_0(f)$ and bottom $S(f)$ horizons (Figure 3c), we calculate Q via linear regression with frequency f using the form,

$$\ln\left(\frac{S(f)}{S_0(f)}\right) = -\frac{\pi \Delta t}{Q} f, \quad (6)$$

where Δt is the traveltime separating the two horizons (Figure 3d). For all traces at Blake Ridge, we perform this regression over $45\ \text{Hz} \le f \le 125\ \text{Hz}$, whereas at Finneidfjord, we use $20\ \text{Hz} \le f \le 250\ \text{Hz}$. This method assumes a constant Q over these frequency bands, which we chose because they contain most of the seismic energy. We denote this estimate as $\hat{Q}$ throughout the rest of this paper.

Attenuation model inversion

The inversion discussed in this section refers to the mathematical inversion of a function (the attenuation model), rather than a seismic inversion for the impedance or velocity from the full traces. The inversion performed here uses the measured attenuation $\hat{Q}$ as data for the model output and infers values for the model parameters of interest, namely gas saturation. Because of the complexity of the attenuation model, the mathematical inversion is performed with a genetic algorithm, which is a stochastic optimization technique that "evolves" an initial guess of the model parameter values toward a solution that matches the data.

By using the attenuation model of Carcione and Picotti (2006), we assume the gas inhomogeneities are arranged in periodic layers. Although this assumption of gas layers may not be realistic, the work of Dutta and Seri (1979) shows that the attenuation predicted by White's model (and thus the model of Carcione and Picotti [2006]) is not very sensitive to the configuration of gas inclusions. Our assumption of periodic layering may limit the accuracy of our gas saturation estimates, as a model with random layering (e.g., Müller and Gurevich, 2004; Toms et al., 2007) may be more realistic. The inversion described here should work for such a random model, but would require additional (or a substitution of different) parameters to describe the distribution of gas (e.g., via an autocorrelation function).

Table 1. Initial parameter values and parameter limits for Blake Ridge and Finneidfjord.

	Lower bound	Initial value	Upper bound
	Global (both sites)		
Gas saturation S_g (%)	0	1	100
Porosity φ	0.38[a]	0.55	0.73[a]
Permeability κ (darcy)	10^{-8}[a]	10^0	10^5[a]
Solid grain bulk modulus K_s (GPa)	20[b]	30	70[b]
Solid grain shear modulus μ_s (GPa)	5[b]	13	50[b]
Solid grain density ρ_s (g/cm^3)	2.55[b]	2.65	2.71[b]
Water bulk modulus K_w (GPa)	2.00	2.25[c]	2.50
Water density ρ_w (g/cm^3)	1.000	1.025	1.030
Water viscosity η_w (Pa · s)	0.001	0.003[c]	0.005
Gas viscosity η_g (10^{-4} Pa · s)	1.0	1.5[c]	2.0
	Blake Ridge		
Total pressure P (MPa)	~32.41	~32.93	~35.19
Temperature T (°C)	11	12	16
Layer thickness d (m)	70	75	80
	Finneidfjord		
Total pressure P (MPa)	~0.55	~0.77	~2.93
Temperature T (°C)	0	5	10
Layer thickness d (m)	36.5	37.5	38.5

[a]Schon (1996)
[b]Mavko (1998)
[c]Carcione and Picotti (2006)

Our goal in this section is to find the parameter set,

$$\theta = \{S_g, \phi, \kappa, K_s, \mu_s, \rho_s, K_w, \rho_w, \eta_w, \eta_g, P, T, d\}, \quad (7)$$

that matches the modeled quality factor $Q(\theta)$ from Carcione and Picotti (2006) with the effective quality factor estimates $\hat{Q}$ from the previous section (see Table 1 for the list of the 13 parameters belonging to θ, and see Appendix A for the model that defines $Q(\theta)$). Our estimates of $\hat{Q}$ from the previous section assume a constant Q, whereas Carcione and Picotti (2006) model frequency-dependent Q. Over our frequency bands (20–150 Hz for Blake Ridge, and 40–500 Hz for Finneidfjord), this modeled Q is approximately linear with frequency, and so we take the minimum Q (maximum attenuation) calculated over our frequency bands as $Q(\theta)$ (Figure 4). To get our parameter estimates ($\hat{\theta}$), we solve

$$\hat{\theta} = \underset{\theta \in \Re^{13}}{\arg\min}\, \delta(\theta), \quad (8)$$

where

$$\delta(\theta) = |\hat{Q} - Q(\theta)|. \quad (9)$$

We use a genetic algorithm to estimate $\hat{\theta}$ because this class of algorithms is particularly well suited for optimizing (multidimensional) nonlinear equations that may not be globally concave (Sambridge and Drijkoningen, 1992), such as the system of equations in Carcione and Picotti (2006) (Appendix A).

Genetic algorithms rely on random sampling from populations of the input parameters in θ. Here, we define the parameters as uniformly distributed with lower and upper limits listed in Table 1, so our inversion becomes a constrained optimization problem. We choose the lower and upper limits based on our a priori understanding of the likely geologic conditions at each of the two locations.

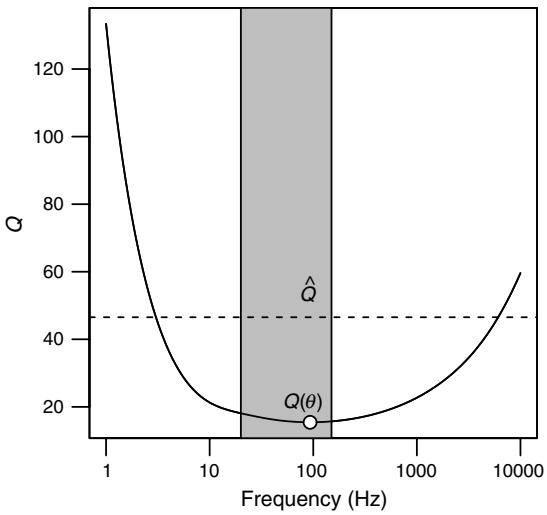

Figure 4. The frequency-dependency of the modeled $Q(\theta)$ (solid curve) for trace 869, using the initial parameter values in Table 1. The dashed line represents the estimated $\hat{Q}$ from Figure 3, and the shaded grey area is the relevant frequency range for the seismic survey at Blake Ridge. The goal of the inversion is to adjust the parameters θ such that the minima of the $Q(\theta)$ curve in the frequency range (white circle) falls on the dashed line.

We base this a priori knowledge on typical reference values for seawater, methane, and a wide variety of offshore sediment types (Schön, 1996; Mavko et al., 1998; Carcione and Picotti, 2006). Pressures reported here are mean values across the profiles, where the lower pressure is the hydrostatic pressure at the top of the gas-bearing layer (assuming $V_P = 1500$ m/s), the upper pressure is the hydrostatic pressure at the bottom plus 2 MPa, and the initial value is the mean of the two hydrostatic values plus 1% of the overburden pressure based on ρ_s. Note that layer thickness is determined from the seismic profiles as well. Therefore, the range between the lower and upper limits reflects the degree of uncertainty in our understanding of the true in situ values.

The initial values in Table 1 represent a first guess of θ and are not required to start the genetic algorithm, but help direct the algorithm to likely optimal parameters. It should be noted that the final results are theoretically not significantly sensitive to these initial values because the algorithm randomly searches over the global parameter space. Of far greater importance is the choice of the lower and upper limits defining each parameter's distribution. In reference to Figure 5, we call our initial guess θ_1, and it is included in the initial sample population (at generation $m = 0$), which is randomly generated using the uniform distributions of the parameters. We limit all our population sizes to $n = 5000$ individual parameter sets. We determine the fitness of these individuals by the objective function, equation 9, and select an arbitrary number of the best individuals to parent, and be included in (or cloned into), the next generation. New individuals of the next generation are generally created in two different ways: by crossover, where one or more parameters are combined between two parents, and by mutation, where one or more parameters of a parent are randomly altered based on the uniform parameter distributions. The fitness of the new generation is then evaluated, and this loop continues for $m = 200$ generations (or terminates early if there is no significant change in δ over 10 generations), at which point the best individual is returned. Because the best individual from each generation is cloned into the subsequent generation, the individual returned at the end is guaranteed to be the best individual from the entire $m = 200$ generations.

Genetic algorithms have been shown to be highly successful at getting the objective function (e.g., $\delta(\theta)$) in the local neighborhood of the global minimum, but perform poorly when it comes to localized optimization. Coupling the genetic algorithm with a gradient search method overcomes this deficiency. We run a quasi-Newton search routine on the best individual at the end of each of the final 10 generations to push the lowest $\delta(\theta)$ returned from the genetic algorithm arbitrarily closer to the locally minimum $\delta(\hat{\theta})$, which is most likely also the global minimum by that point in the algorithm. This entire process (GA and quasi-Newton) is implemented with the *genoud* function of the package *rgenoud* (Mebane Jr. and Sekhon, 2011) for the statistical software R (R Development Core Team, 2009).

One important step that we add to the model inversion deals with the convex relationship that $Q(S_g, \hat{\phi}, \hat{\kappa}, \hat{K}_s, \hat{\mu}_s, \hat{\rho}_s, \hat{K}_w, \hat{\rho}_w, \hat{\eta}_w, \hat{\eta}_g, \hat{P}, \hat{T}, \hat{d})$ has with S_g (Lee and Collett, 2009; Carcione et al., 2003). This relationship is inherent to the model of White (1975), which is in turn adopted in Carcione and Picotti (2006). Figure 6 illustrates this relationship, using the trace closest to hole 997 at Blake Ridge as an example (trace 869) and parametrizing the curve with our final estimated $\hat{\theta}$ for that location. For our estimated $\hat{Q} = 46.5$ (represented by the dashed line), there exist two possible S_g

values (i.e., there exist two global minima of $\delta(S_g, \hat{\phi}, \hat{\kappa}, \hat{K}_s, \hat{\mu}_s, \hat{\rho}_s, \hat{K}_w, \hat{\rho}_w, \hat{\eta}_w, \hat{\eta}_g, \hat{P}, \hat{T}, \hat{d})$). By solving for the roots of this $\delta(S_g)$ (the absolute difference between this curve and the dashed line) and taking the minimum root, we force the selection of the smallest S_g that yields a matching $Q(\theta)$ (the open circle in Figure 6). The genetic algorithm alone would essentially randomly sample from the set of roots. A discussion for the justification of taking the smaller of the two roots is provided in the "Discussion" section.

RESULTS

Here, we use Blake Ridge to validate the procedure outlined above because of the logging data that penetrates the gas-bearing layer at the three boreholes along the seismic line (Figure 1). We show that our estimates of S_g from the genetic algorithm inversion of the P-wave attenuation model are similar to measured S_g values from resistivity logs and pressure core samples from Blake Ridge (such data are described in Collett and Ladd, 2000; Tinivella and Lodolo, 2000; Lu and McMechan, 2002). We also demonstrate the ability of our method to detect low levels of gas saturation within the shallow free gas deposit at Finneidfjord.

Blake Ridge

Figure 7 summarizes the attenuation measurement and gas saturation inversion at Blake Ridge. Figure 7b shows a general trend of decreasing $\hat{Q}$ from left to right, and the values immediately to the right of hole 997 (at trace 869) show relatively homogenous, high attenuation (low Q). In general, the relative values of $\hat{Q}$ are what we expect given the amplitudes associated with the bottom horizon; larger $\hat{Q}$ values occur where the bottom horizon coincides with stronger, more continuous reflections (e.g., between holes 994 and 995), and lower where it is underlain by more chaotic reflections (Figure 7). Despite the flattening and stacking of the seismic data, our $\hat{Q}$ still show some erratic changes along the profile. Also, we removed 71 values of $\hat{Q} \leq 0$, leaving 740 observations out of the original 811 traces.

Our measured $\hat{Q}$ values more or less agree with values from Wood (2000), who observes $Q = 200$ to 300 around trace 1400, $Q = 30$ to 50 at hole 995 (trace 1297), and $Q = 70$ to 150 at hole 997 (trace 869) and further right. This third range constitutes the greatest discrepancy between the Q values of Wood (2000) and those of this study, which estimates significantly lower values ($\hat{Q} \approx 6$ to 143).

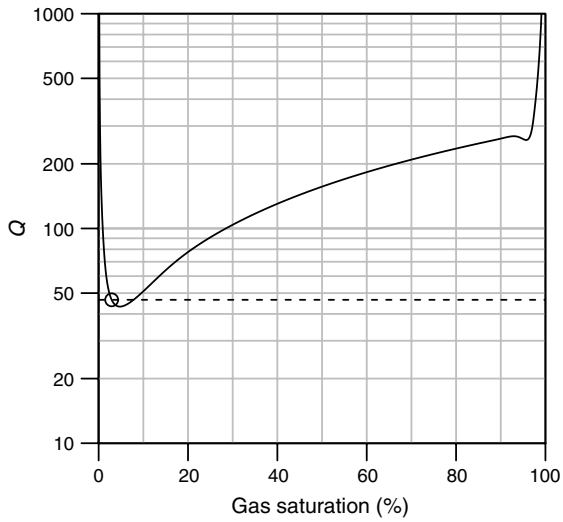

Figure 6. For trace 869 (closest to hole 997) at Blake Ridge, a plot of $Q(\theta)$ versus S_g, with the other 12 parameters in θ set to their values in $\hat{\theta}$ returned by the genetic algorithm inversion. The open circle represents the minimum S_g that gives $\delta(S_g, \hat{\phi}, \hat{\kappa}, \hat{K}_s, \hat{\mu}_s, \hat{\rho}_s, \hat{K}_w, \hat{\rho}_w, \hat{\eta}_w, \hat{\eta}_g, \hat{P}, \hat{T}, \hat{d}) = 0$. The dashed line represents $\hat{Q} = 46.5$ for this trace.

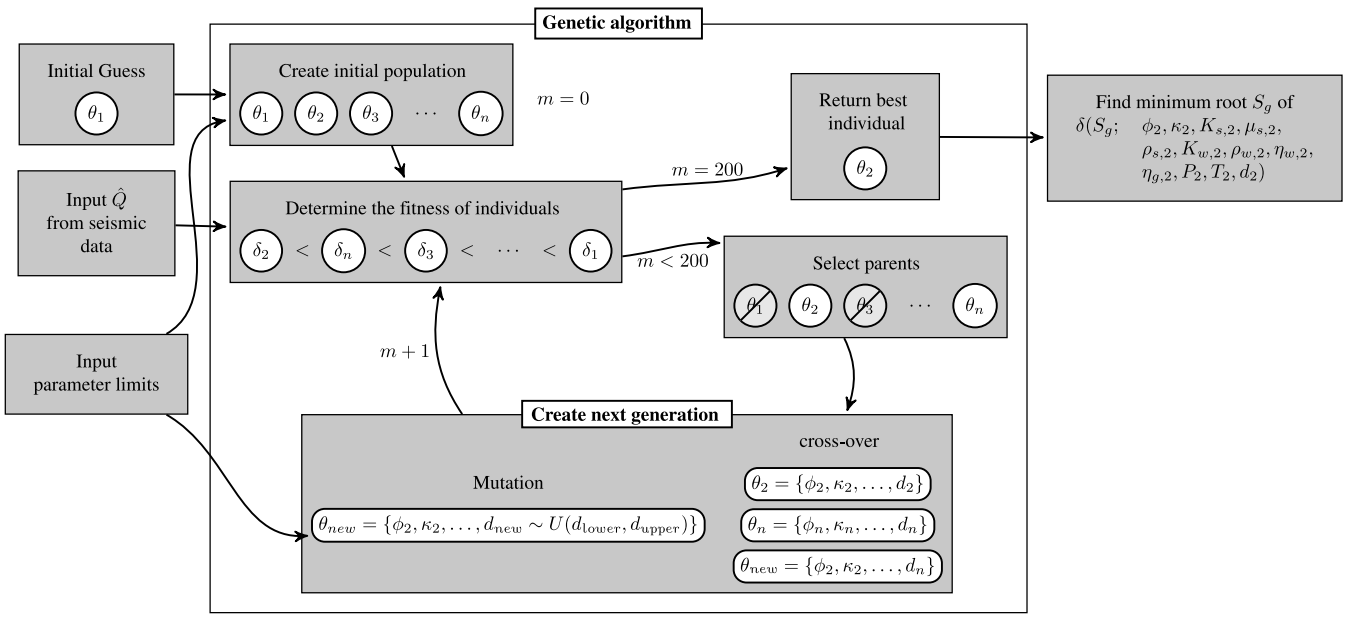

Figure 5. A simplified flowchart representation of the genetic algorithm for finding $\hat{Q}$ that minimizes $\delta(\theta)$ (i.e., matches $Q(\theta)$ to $\hat{Q}$). In this example, $\theta_2 = \hat{\theta}$.

The gray line in Figure 7b represents the $Q(\theta)$ returned from the genetic algorithm, which effectively agree with our measured $\hat{Q}$ in all cases ($0 \leq \delta \leq 4e-12$). These low δ values indicate that the genetic algorithm converged on a solution in all cases. By inspection of Figure 7b and c, we can see that lower $\hat{Q}$ values generally produce higher S_g values, or, in the forward sense, more gas causes greater attenuation, which is what we expect from Figure 6 up to a certain S_g (i.e., following the curve left of the vertex).

Finneidfjord

We demonstrate the applicability of our method to other environments by examining the shallow free gas zone at Finneidfjord, Norway. In Figure 8b, we can see that our $\hat{Q}$ vary much more smoothly across the profile than at Blake Ridge, owing primarily to the relative lack of noise in the Finneidfjord seismic surveys, but also to the shorter profile length and shorter shotpoint spacing. A further consequence of this lack of noise is that all $\hat{Q} > 0$, and so no values were pruned from these results, unlike at Blake Ridge. As with the results from Blake Ridge, $Q(\theta)$ here (gray line in Figure 8b) agrees nearly perfectly to our measured $\hat{Q}$ ($0 \leq \delta \leq 6e-15$). Comparing Figure 8a to Figure 8b, lower $\hat{Q}$ values (higher P-wave attenuation) generally occurs with smaller seismic amplitudes at the lower horizon (i.e., with more amplitude blanking), as we would expect. It is also reassuring to see that $\hat{Q}$ increase toward the edges of this gas zone, especially at the left side, where strong reflectors at depth are truncated by the amplitude blanking of the gas zone.

We also see at Finneidfjord the general increase in S_g with the decrease in $\hat{Q}$: the mean S_g increases from ~0.03% to the right of trace 140 to ~0.09% to the left of trace 140, while mean $\hat{Q}$ values decrease from ~31 to ~14, respectively. Comparing our results from Blake Ridge to those at Finneidfjord, we see a modest decrease in the mean $\hat{Q}$ (across the entirety of each profile) from ~72 to ~23, respectively, whereas we see a dramatic decrease in mean S_g of two orders of magnitude: from ~6.304% to ~0.063%.

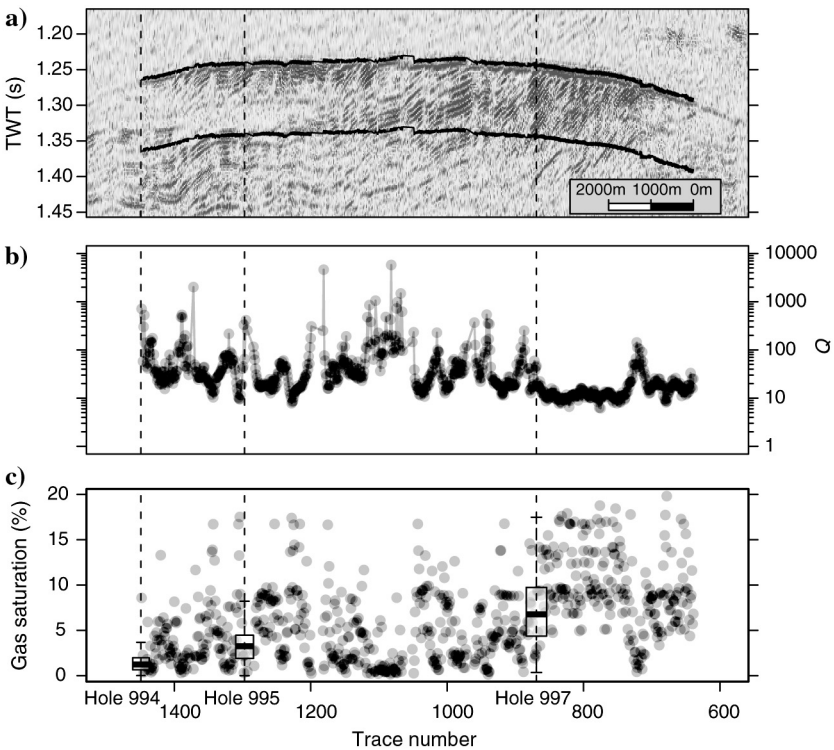

Figure 7. Blake Ridge USGS line 01 seismic profile (a) with horizon picks in black lines, results for our $\hat{Q}$ measurements (b), where the grey line represents the final $Q(\theta)$ returned by the genetic algorithm, and S_g results from the model inversion (c). The points in these plots are transparent to visualize the density of values (more overlapping points give a darker shade). Boxplots represent the distribution of S_g estimates based on resistivity logs from holes 994, 995, and 997 (closest to traces 1449, 1297, and 869, respectively).

DISCUSSION

Here, we compare our estimates of S_g with those from resistivity logs collected on ODP Leg 164, and from previous studies, all of which are summarized graphically in Figure 9. Our estimates generally agree with the S_g estimates from resistivity logs. We use the same empirical relation for deriving S_g from resistivity as in Lu and McMechan (2002), i.e.,

$$S_g = 1 - \left(\frac{R_0}{R_t}\right)^{\frac{1}{n}}, \tag{10}$$

where

$$R_0 = 0.8495 + (2.986 \times 10^{-4})Z, \tag{11}$$

R_t is the measured resistivity, Z is the depth below the sea floor (in meters), and $n = 1.62$ for free gas. Plotting our estimates of S_g from the closest 25 seismic traces to each of the three boreholes provides a visual comparison of the central tendency of each distribution (here it is the median) as well as the spread of values between our estimates and those from the resistivity logs.

Our S_g estimates returned by the genetic algorithm inversion generally agree with those of previous studies from Blake Ridge. General estimates of S_g that characterize the whole layer beneath the BSR range from ~1% (Holbrook et al. [1996], from velocity analysis) to ~12% (Dickens et al. [1997], from pressure core samples at holes 995 and 997). Using a multichannel seismic line that runs perpendicular to the profile used in our analysis, Ecker et al. (2000) and Lu and McMechan (2004) find similar values in this area: 1%–2% and 1%–8%, respectively. Lu and McMechan (2002) estimate the distribution of free gas within three layers beneath the BSR, and report ranges of 11%–14% for the uppermost layer, 7%–11% at further depth, and 1%–2% even deeper (however, this third layer lies beneath the layer examined in our analysis). They report that the highest saturations exist at hole 997, and from visual inspection of their figures, next to no gas exists at hole 994. Tinivella and Lodolo (2000) estimate 4% free gas at hole 997, <1% at 995, and no free gas at 994. Discrepancies between our estimates and those of other

studies and resistivity logs may be due to changes in S_g with depth. Although our estimates represent an average S_g through the thickness of the layer, the resistivity boxplots in Figure 9 summarize many recordings at specific depths throughout the thickness of this layer. Similarly, the literature discussed above provides estimates that may only represent subsections of the layer in our analysis.

The results from Finneidfjord show that the inversion of the attenuation model is sensitive to very low gas saturations. Besides relying on other measurements to achieve reliable gas-saturation estimates (Lee, 2004), P-wave velocity analysis requires highly accurate measurements of V_P to get precise estimates of S_g (Zillmer, 2006). Lee and Collett (2009) show that, within the seismic frequency range, changes in quality factor Q far exceed (by orders of magnitude) changes in V_P with respect to large changes in gas saturation. Over lower gas saturations, P-wave quality factor still varies more dramatically than velocity, suggesting that Q is a better metric for inverting for S_g.

Although our $\hat{Q}$ at Finneidfjord are generally lower than at Blake Ridge, our resulting estimates of S_g are also lower (Figure 8), but we would expect a greater degree of gas saturation to accompany a greater degree of attenuation when only considering the minimum root of $\delta(S_g)$ (e.g., below $S_g \approx 5\%$ in Figure 6). This makes sense when considering the large contrast in ambient pressure (and, to a lesser degree, temperature) between these two environments in the context of equation A-2. The smaller pressure at Finneidfjord reduces the density of the free gas. Less dense gas is more compressible and thus more capable of producing higher levels of P-wave attenuation. As noted in Carcione and Picotti (2006), the more compliant fluid in the sediment's pore space largely controls the amount of attenuation. This relationship is illustrated in Figure 10, where contours of equal Q are plotted as a function of S_g and P, with all other parameters in θ held as the returned values in $\hat{\theta}$ from trace 140 and Finneidfjord. As pressure decreases, any given Q can be explained by either smaller or larger S_g.

In reference to Figure 6, taking the smaller of the two roots of $\delta(S_g)$ ensures small S_g values that agree with the gas bubble saturation that is found in free gas deposits, typically less than ~10% (Holbrook et al., 1996; Haacke et al., 2007). Observations from cores at Blake Ridge and Finneidfjord report gas in discrete bubble form, as opposed to entire sections of sediment purely saturated with gas. Note that from Figure 6, larger Q can only be explained with more disparate S_g values, whereas the roots at smaller Q are not as different. Figure 10 shows that the difference between the S_g roots is also a function of pressure, where lower pressures create larger differences between the roots for a given Q. On a side note, an alternative to taking the smaller of the two roots would be to report both S_g roots, and the user could select which set of S_g, the minimum or maximum, is more realistic over the particular profile.

Additionally, because the genetic algorithm fundamentally relies on random sampling of the parameter distributions, it does introduce some noise into the S_g estimates. Whereas traditional inversion techniques would provide a unique mapping from the observations (e.g., $\hat{Q}$) to the parameter(s) (e.g., θ), the high nonlinearity of the attenuation model used here, as well as the use of constrained versus known

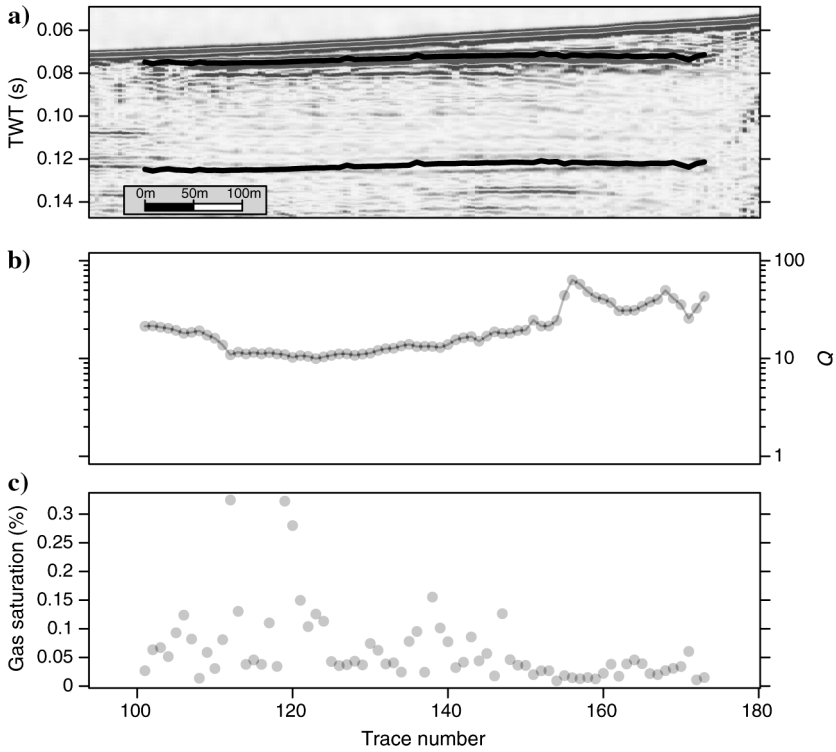

Figure 8. Results for Finneidfjord, Norway, including (a) line 08 seismic profile (with horizon picks in black lines), (b) resulting $\hat{Q}$ measurements (where the grey line indicates the final $Q(\theta)$ from the genetic algorithm inversion), and (c) S_g results from the inversion. See Figure 2 for map of line 08.

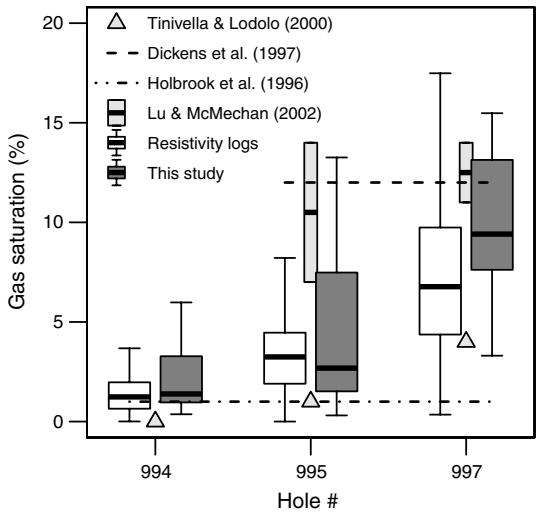

Figure 9. Boxplots of S_g estimates from resistivity logs at each hole (white) plotted alongside boxplots of our 25 closest S_g estimates to each hole (gray). For clarity, outliers are not plotted along with the boxplots but are used in the calculation of the boxplots.

parameter values, make such a mapping infeasible. The genetic algorithm randomly identifies this mapping, and as such, the relationship between $\hat{Q}$ and S_g will differ from trace to trace. As the inverse of the S/N, the coefficient of variation gives us a sense of how much random noise is introduced by the genetic algorithm. The coefficient of variation is the ratio of the standard deviation to the mean, and here we calculate the mean and standard deviation of the natural logarithm of $\hat{Q}$ and S_g because these values are theoretically bounded at zero and their distributions appear more lognormal than normal. For the results from Blake Ridge and Finneidfjord, the S/N of $\hat{Q}$ is 3.46 and 5.80, respectively, whereas that of S_g is 1.52 and 3.92. Thus, our genetic algorithm inversion puts roughly twice as much noise in the resulting S_g estimates as the ingoing $\hat{Q}$ values.

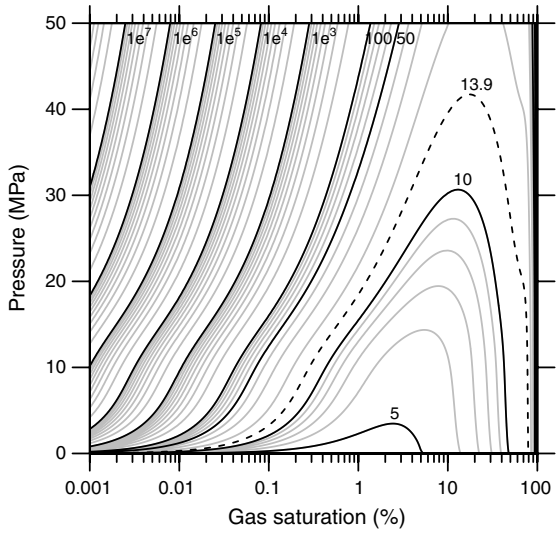

Figure 10. Contours of equal Q plotted against S_g and P show that the same level of P-wave attenuation at smaller pressure can be achieved with significantly less gas. The other 11 parameters used to calculate these contours were taken from the $\hat{\theta}$ of trace 140 at Finneidfjord, and the dashed contour marks the $\hat{Q}$ for this same trace.

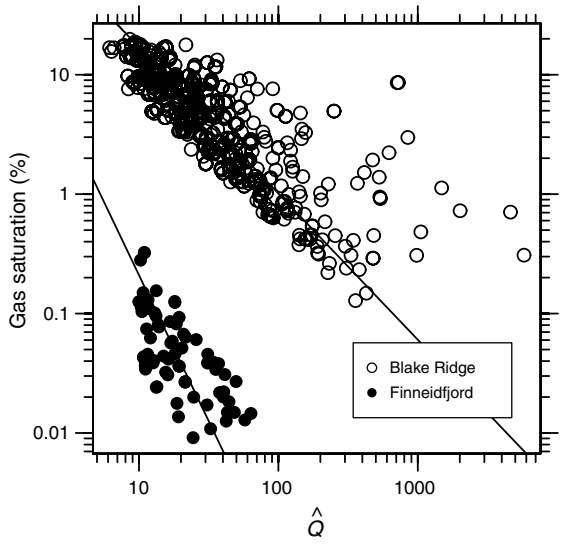

Figure 11. Plot showing the linearity between the natural logarithms of S_g and $\hat{Q}$ at the two sites in this study. Lines represent linear regressions to each set of data points, and serve to illustrate the general decreasing trend of S_g with increasing $\hat{Q}$.

That being said, Figure 11 shows that S_g monotonically decreases with $\hat{Q}$, and that the noise produced by the genetic algorithm does not dramatically obscure the mapping of $\hat{Q}$ to S_g. Larger values of $\hat{Q}$ tend to produce estimates of S_g with greater deviation from the linearly decreasing trends suggested by the regression lines in Figure 11. The potential for error in the spectral ratio estimates of $\hat{Q}$ (which would then propagate into the inversion) certainly exists, but cannot readily be assessed quantitatively because we do not know the true Q values at these sites. Noting that the deviation of the S_g for these larger Q tends to be above the regression line, especially in the Blake Ridge case, one potential limitation of the genetic algorithm inversion may lie in convergence to very low gas saturation values, including $S_g = 0$. Regardless of such limitations, the estimates of S_g from this inversion are still informative and reasonably accurate (Figure 9).

CONCLUSION

In this paper, we demonstrate the feasibility of obtaining a reasonably good first-order estimate of the distribution of gas saturation strictly from seismic reflection survey data and generally accepted values of material properties. Our proposed inversion method relies on a model of P-wave attenuation, which shares a stronger relationship to the hydraulic properties of a geologic medium than velocity. Inverting the P-wave attenuation model with a genetic algorithm allows us to supply ranges of model parameter values instead of exact measurements. These ranges reflect likely conditions within the layer of interest, and can be established from literature or the seismic survey (e.g., layer thickness). The genetic algorithm efficiently searches over this parameter space for the set of parameter values that produces the observed level of attenuation within the seismic survey frequencies.

Our resulting estimates of gas saturation not only agree with estimates of previous studies at Blake Ridge, but also with estimates from resistivity logs collected on ODP Leg 164. Although the variance in our predictions is high, so is the variance in these previous S_g measurements and predictions. The random noise generated by the genetic algorithm does not make our estimates significantly different than those of the previous studies and resistivity logs. Furthermore, our example at Finneidfjord demonstrates the generalizability of this method to shallower environments that have lower levels of pressure and gas saturation. Although in this paper we only demonstrate the inversion of the P-wave attenuation model with the genetic algorithm using single-channel seismic data, our method should work for other forms of seismic acquisition (e.g., 3D surveys) as long as the data are processed in such a way as to not preclude realistic quality factor estimates.

ACKNOWLEDGMENTS

We thank Tommy Rasmussen and Lars Zühlsdorff (NORSAR) for their help processing the Finneidfjord seismic data set, as well as two anonymous reviewers for their thoughtful and constructive feedback. Further thanks is given to Bill Dillon (USGS, Woods Hole) for providing the Blake Ridge seismic profile data. Seismic Microtechnologies graciously provided us with an education user license for their KINGDOM software, which was used for interpretation of the seismic profiles at both sites in this paper. This

is paper no. 375 from the International Centre for Geohazards, Oslo, and funding for this research was provided by NSF grant OISE-0530151.

APPENDIX A

MODEL OF P-WAVE ATTENUATION IN PARTIALLY SATURATED MARINE SOILS

The following specifies the system of equations used in the genetic algorithm optimization routine presented in the "Methods" section. This appendix nearly reproduces the model introduced by Carcione and Picotti (2006), with some minor adjustments to put the equations in the framework of a minimization problem (see equation 8). We urge our audience to read Carcione and Picotti (2006) to more fully understand the features of this model.

Because in situ methane behaves as a real gas, for a given gas pressure P (Pa) and temperature T (°C) above the critical temperature of −82.7°C, we can solve the van der Waals equation,

$$(P + A\rho_g^2)(1 - B\rho_g) = \rho_g R(T + 273), \tag{A-1}$$

for gas density $\rho_g(\mathrm{kg/m^3})$. Here, $R = 519.4\ \mathrm{J/(kg°K)}$, $A = 879.9\ \mathrm{Pa(m^3/kg)^2}$, and $B = 2.675 \times 10^{-3}\ \mathrm{m^3/kg}$. Using this ρ_g, we can find the bulk modulus for gas:

$$K_g = \frac{4}{3}\left[\frac{\rho_g R(T + 273)}{(1 - B\rho_g)^2} - 2A\rho_g^2\right]. \tag{A-2}$$

For known porosity ϕ, solid grain bulk modulus K_s and solid grain shear modulus μ_s, the dry-rock bulk and shear moduli are

$$K_m = K_s(1 - \phi)^{4/(1-\phi)}, \tag{A-3}$$

and

$$\mu_m = K_m\mu_s/K_s, \tag{A-4}$$

respectively. The Gassmann modulus K_G is found as

$$K_G = K_m + \alpha^2 M, \tag{A-5}$$

where

$$\alpha = 1 - \frac{K_m}{K_s} \tag{A-6}$$

and

$$M = \frac{K_s}{1 - \phi - K_m/K_s + \phi K_s/K_f}. \tag{A-7}$$

The bulk fluid modulus $K_f = K_w$ for the water-saturated sublayer and $K_f = K_g$ for the gas-saturated sublayer. Here, we consider a system of layered porous media and denote the water-saturated sublayer with subscript 1 and the gas-saturated sublayer with subscript 2. These sublayers have thicknesses d_1 and d_2, respectively, and $d = d_1 + d_2$. Furthermore, $S_g = d_2/d * 100\%$.

The complex bulk modulus is

$$E = \left[\frac{1}{E_0} + \frac{2(r_2 - r_1)^2}{i\omega(d_1 + d_2)(I_1 + I_2)}\right]^{-1}, \tag{A-8}$$

where i is the imaginary unit, ω is angular frequency, and

$$E_0 = \left(\frac{p_1}{E_{G_1}} + \frac{p_2}{E_{G_2}}\right)^{-1}, \tag{A-9}$$

with $p_j = d_j/(d_1 + d_2)$ and $E_{G_j} = K_{G_j} + \frac{4}{3}\mu_m$ for $j = 1, 2$. Furthermore, omitting the subscript i for clarity, the ratio of fast P-wave fluid tension to total normal stress is

$$r = \frac{\alpha M}{E_G}, \tag{A-10}$$

and the impedance related to the slow P-wave is

$$I = \frac{\eta}{\kappa k}\coth\left(\frac{kd}{2}\right), \tag{A-11}$$

where the slow P-wave complex number is

$$k = \sqrt{\frac{i\omega\eta}{\kappa K_E}}, \tag{A-12}$$

the effective modulus is

$$K_E = \frac{E_m M}{E_G}, \tag{A-13}$$

and the dry-rock fast P-wave modulus is

$$E_m = K_m + \frac{4}{3}\mu_m. \tag{A-14}$$

With the average density $\bar{\rho} = p_1\rho_1 + p_2\rho_2$, and the complex velocity defined by $\bar{\rho}v^2 = E$, we get the loss angle

$$\Theta = \tan^{-1}\left[\frac{\Im(v^2)}{\Re(v^2)}\right], \tag{A-15}$$

with $\Im$ and $\Re$ giving the imaginary and real components, respectively. Finally, we obtain quality factor via

$$Q^{-1} = \tan\Theta. \tag{A-16}$$

Here, we evaluate these equations over the range of $\omega = 2\pi f$ given in the Methods section. We take $Q(\theta)$ as our minimum Q from equation A-16 over this frequency range.

REFERENCES

Archie, G., 1942, The electrical resistivity log as an aid in determining some reservoir characteristics: Journal of Petroleum Technology, **5**, 1–8.

Bangs, N. L. B., D. S. Sawyer, and X. Golovchenko, 1993, Free gas at the base of the gas hydrate zone in the vicinity of the Chile

triple junction: Geology, **21**, 905–908, doi: 10.1130/0091-7613(1993)021<0905:FGATBO>2.3.CO;2.
Berndt, C., J. Mienert, M. Vanneste, and S. Bünz, 2005, Gas hydrate dissociation and sea-floor collapse in the wake of the Storegga Slide, Norway: Norwegian Petroleum Society Special Publications, **12**, 285–292.
Best, A. I., C. R. I. Clayton, O. Longva, and M. Szuman, 2003, The role of free gas in the activation of submarine slides in Finneidfjord: First International Symposium on Submarine Mass Movements and their Consequences, EGS-AGU-EUG Joint Meeting, 491–498.
Biot, M. A., 1962, Mechanics of deformation and acoustic propagation in porous media: Journal of Applied Physics, **33**, 1482–1498, doi: 10.1063/1.1728759.
Bünz, S., J. Mienert, M. Vanneste, and K. Andreassen, 2005, Gas hydrates at the Storegga Slide: Constraints from an analysis of multicomponent, wide-angle seismic data: Geophysics, **70**, no. 5, B19–B34, doi: 10.1190/1.2073887.
Carcione, J. M., H. B. Helle, and N. H. Pham, 2003, White's model for wave propagation in partially saturated rocks: Comparison with poroelastic numerical experiments: Geophysics, **68**, 1389–1398, doi: 10.1190/1.1598132.
Carcione, J. M., and S. Picotti, 2006, P-wave seismic attenuation by slow-wave diffusion: Effects of inhomogeneous rock properties: Geophysics, **71**, no. 3, O1–O8, doi: 10.1190/1.2194512.
Collett, T., and J. Ladd, 2000, Detection of gas hydrate with downhole logs and assessment of gas hydrate concentrations (saturations) and gas volumes on the Blake Ridge with electrical resistivity log data: Proceedings of the Ocean Drilling Program, Scientific Results, **164**, 179–191.
Dickens, G. R., C. K. Paull, and P. Wallace, 1997, Direct measurement of in situ methane quantities in a large gas-hydrate reservoir: Nature (London), **385**, 426–428, doi: 10.1038/385426a0.
Dutta, N. C., and A. J. Seriff, 1979, On White's model of attenuation in rocks with partial gas saturation: Geophysics, **44**, 1806–1812, doi: 10.1190/1.1440940.
Ecker, C., J. Dvorkin, and A. M. Nur, 2000, Estimating the amount of gas hydrate and free gas from marine seismic data: Geophysics, **65**, 565–573, doi: 10.1190/1.1444752.
Gurevich, B., V. B. Zyrianov, and S. L. Lopatnikov, 1997, Seismic attenuation in finely layered porous rocks: Effects of fluid flow and scattering: Geophysics, **62**, 319–324, doi: 10.1190/1.1444133.
Haacke, R. R., G. K. Westbrook, and R. D. Hyndman, 2007, Gas hydrate, fluid flow and free gas: Formation of the bottom-simulating reflector: Earth and Planetary Science Letters, **261**, 407–420, doi: 10.1016/j.epsl.2007.07.008.
Holbrook, W. S., H. Hoskins, W. T. Wood, R. A. Stephen, and D. Lizarralde, 1996, Methane hydrate and free gas on the Blake Ridge from vertical seismic profiling: Science, **273**, 1840–1843, doi: 10.1126/science.273.5283.1840.
Horozal, S., G. H. Lee, B. Y. Yi, D. G. Yoo, K. P. Park, H. Y. Lee, W. Kim, H. J. Kim, and K. Lee, 2009, Seismic indicators of gas hydrate and associated gas in the Ulleung Basin, East Sea (Japan Sea) and implications of heat flows derived from depths of the bottom-simulating reflector: Marine Geology, **258**, 126–138, doi: 10.1016/j.margeo.2008.12.004.
Kayen, R., and H. Lee, 1993, Slope stability in regions of sea-floor gas hydrate: Beaufort Sea continental slope, *in* W. C. Schwab, H. J. Lee, and D. C. Twichell, eds., Submarine landslides; selected studies in the U.S. Exclusive Economic Zone: U.S. Geological Survey Bulletin, 2002, 97–103.
Lee, M. W., 2004, Elastic velocities of partially gas-saturated unconsolidated sediments: Marine and Petroleum Geology, **21**, 641–650, doi: 10.1016/j.marpetgeo.2003.12.004.
Lee, M. W., and T. S. Collett, 2009, Unique problems associated with seismic analysis of partially gas-saturated unconsolidated sediments: Marine and Petroleum Geology, **26**, 775–781, doi: 10.1016/j.marpetgeo.2008.07.009.
Li, H. B., W. Z. Zhao, H. Cao, F. C. Yao, and L. Y. Shao, 2006, Measures of scale based on the wavelet scalogram with applications to seismic attenuation: Geophysics, **71**, no. 5, V111–V118, doi: 10.1190/1.2211529.
Lu, S. M., and G. A. McMechan, 2002, Estimation of gas hydrate and free gas saturation, concentration, and distribution from seismic data: Geophysics, **67**, 582–593, doi: 10.1190/1.1468619.
Lu, S., and G. A. McMechan, 2004, Elastic impedance inversion of multichannel seismic data from unconsolidated sediments containing gas hydrate and free gas: Geophysics, **69**, 164–179, doi: 10.1190/1.1649385.
Mavko, G., T. Mukerji, and J. Dvorkin, 1998, The rock physics handbook: Tools for seismic analysis in porous media: Cambridge University Press.
McAdoo, B. G., M. K. Capone, and J. Minder, 2004, Seafloor geomorphology of convergent margins: Implications for Cascadia seismic hazard: Tectonics, **23**, TC6008, doi: 10.1029/2003TC001570.
McAdoo, B. G., L. Pratson, and D. Orange, 2000, Submarine landslide geomorphology, US continental slope: Marine Geology, **169**, 103–136, doi: 10.1016/S0025-3227(00)00050-5.
Mebane, W. R. Jr., and J. S. Sekhon, 2011, Genetic optimization using derivatives: The rgenoud package for R: Journal of Statistical Software, **42**, no. 11, 1–26.
Müller, T. M., and B. Gurevich, 2004, One-dimensional random patchy saturation model for velocity and attenuation in porous rocks: Geophysics, **69**, 1166–1172, doi: 10.1190/1.1801934.
Müller, T. M., B. Gurevich, and M. Lebedev, 2010, Seismic wave attenuation and dispersion resulting from wave-induced flow in porous rocks — A review: Geophysics, **75**, no. 5, 75A147–75A164, doi: 10.1190/1.3463417.
Payne, S., M. Worthington, N. Odling, and L. West, 2007, Estimating permeability from field measurements of seismic attenuation in fractured chalk: Geophysical Prospecting, **55**, 643–653, doi: 10.1111/gpr.2007.55.issue-5.
Percival, D. B., and A. T. Walden, 2000, Wavelet methods for time series analysis: Cambridge University Press, Series in statistical and probabilistic mathematics.
Pride, S. R., J. G. Berryman, and J. M. Harris, 2004, Seismic attenuation due to wave-induced flow: Journal of Geophysical Research, **109**, B01201, doi: 10.1029/2003JB002639.
Quan, Y., and J. M. Harris, 1997, Seismic attenuation tomography using the frequency shift method: Geophysics, **62**, 895–905, doi: 10.1190/1.1444197.
R Development Core Team, 2009, R: A language and environment for statistical computing: R Foundation for Statistical Computing, http://www.R-project.org/.
Reine, C., M. van der Baan, and R. Clark, 2009, The robustness of seismic attenuation measurements using fixed- and variable-window time-frequency transforms: Geophysics, **74**, no. 2, WA123–WA135, doi: 10.1190/1.3043726.
Sambridge, M., and G. Drijkoningen, 1992, Genetic algorithms in seismic waveform inversion: Geophysical Journal International, **109**, 323–342, doi: 10.1111/gji.1992.109.issue-2.
Sams, M. S., J. P. Neep, M. H. Worthington, and M. S. King, 1997, The measurement of velocity dispersion and frequency-dependent intrinsic attenuation in sedimentary rocks: Geophysics, **62**, 1456–1464, doi: 10.1190/1.1444249.
Schön, J., 1996, Physical properties of rocks: Fundamentals and principles of petrophysics, Handbook of geophysical exploration: Seismic exploration: Pergamon.
Seifert, A., S. Stegmann, T. Morz, M. Lange, T. Wever, and A. Kopf, 2008, In situ pore-pressure evolution during dynamic CPT measurements in soft sediments of the western Baltic Sea: Geo-Marine Letters, **28**, 213–227, doi: 10.1007/s00367-008-0102-x.
Sills, G. C., S. J. Wheeler, S. D. Thomas, and T. N. Gardner, 1991, Behavior of offshore soils containing gas-bubbles: Geotechnique, **41**, 227–241, doi: 10.1680/geot.1991.41.2.227.
Spencer, T. W., J. R. Sonnad, and T. M. Butler, 1982, Seismic Q — Stratigraphy or dissipation: Geophysics, **47**, 16–24, doi: 10.1190/1.1441275.
Stainsby, S. D., and M. H. Worthington, 1985, *Q* estimation from vertical seismic profile data and anomalous variations in the central North Sea: Geophysics, **50**, 615–626, doi: 10.1190/1.1441937.
Sultan, N., P. Cochonat, J. P. Foucher, and J. Mienert, 2004, Effect of gas hydrates melting on seafloor slope instability: Marine Geology, **213**, 379–401, doi: 10.1016/j.margeo.2004.10.015.
Tinivella, U., and F. Accaino, 2000, Compressional velocity structure and Poisson's ratio in marine sediments with gas hydrate and free gas by inversion of reflected and refracted seismic data (South Shetland Islands, Antarctica): Marine Geology, **164**, 13–27, doi: 10.1016/S0025-3227(99)00123-1.
Tinivella, U., and E. Lodolo, 2000, The Blake Ridge bottom-simulating reflector transect: Tomographic velocity field and theoretical model to estimate methane hydrate quantities: Proceedings of the Ocean Drilling Program, Scientific Results, **164**, 273–281.
Toms, J., T. M. Müller, and B. Gurevich, 2007, Seismic attenuation in porous rocks with random patchy saturation: Geophysical Prospecting, **55**, 671–678, doi: 10.1111/gpr.2007.55.issue-5.
Trehu, A. M., and E. R. Flueh, 2001, Estimating the thickness of the free gas zone beneath Hydrate Ridge, Oregon continental margin, from seismic velocities and attenuation: Journal of Geophysical Research, Solid Earth and Planets, **106**, 2035–2045, doi: 10.1029/2000JB900390.
Trehu, A. M., D. S. Stakes, C. D. Bartlett, J. Chevallier, R. A. Duncan, S. K. Goffredi, S. M. Potter, and K. A. Salamy, 2003, Seismic and seafloor evidence for free gas, gas hydrates, and fluid seeps on the transform margin offshore Cape Mendocino: Journal of Geophysical Research, Solid Earth and Planets, **108**, no. B5, 2263, doi: 10.1029/2001JB001679.
Urgeles, R., B. De Mol, C. Liquete, M. Canals, M. De Batist, J. E. Hughes-Clarke, D. Amblas, P. A. Arnau, A. M. Calafat, J. L. Casamor, V. Centella, K. De Rycker, J. Fabres, J. Frigola, S. Lafuerza, G. Lastras, A. Sanchez, D. Zuniga, W. Versteeg, and V. Willmott, 2007, Sediment undulations on the Llobregat prodelta: Signs of early slope instability or sedimentary

bedforms?: Journal of Geophysical Research, Solid Earth and Planets, **112**, B05102, doi: 10.1029/2005JB003929.
White, J. E., 1975, Computed seismic speeds and attenuation in rocks with partial gas saturation: Geophysics, **40**, 224–232, doi: 10.1190/1.1440520.
Wood, W. T., 2000, In situ measurements of P-wave attenuation in the methane hydrate- and gas-bearing sediments of the Blake Ridge: Proceedings of the Ocean Drilling Program, Scientific Results, **164**, 265–272.
Xu, W. Y., and L. N. Germanovich, 2006, Excess pore pressure resulting from methane hydrate dissociation in marine sediments: A theoretical approach: Journal of Geophysical Research, Solid Earth and Planets, **111**, B01104, doi: 10.1029/2004JB003600.
Yang, S., and J. Gao, 2008, Seismic quality factors estimation from spectral correlation: Geoscience and Remote Sensing Letters, **5**, 740–744, doi: 10.1109/LGRS.2008.2004507.
Zillmer, M., 2006, A method for determining gas-hydrate or free-gas saturation of porous media from seismic measurements: Geophysics, **71**, no. 3, N21–N32, doi: 10.1190/1.2192910.